X-ray-absorption study of CuBr at high pressure

J. M. Tranquada
Brookhaven National Laboratory, Upton, New York 11973-5000

R. Ingalls
Department of Physics (FM-15), University of Washington, Seattle, Washington 98195
(Received 31 March 1986)

The x-ray-absorption spectrum of cuprous bromide has been measured as a function of pressure. The x-ray-absorption near-edge structure proved to be an excellent indicator of high-pressure phase transitions in this material. The normalized "white-line" peak heights at both the Cu and Br K edges decreased on entering the tetragonal phase and increased in going to the NaCl structure. The zinc-blende to tetragonal phase transition took place over a very narrow pressure range centered at 46 ± 5 kbar. The transformation from the tetragonal to the NaCl structure, on the other hand, showed a broad mixed-phase region, suggesting a nucleation-and-growth mechanism for the transition. The mixed-phase region was centered at 75 ± 6 kbar. No evidence of a phase between the zinc-blende and tetragonal phases was observed, presumably because it does not exist. Analysis of the extended x-ray-absorption fine-structure (EXAFS) clearly showed that there is no change in coordination in going from the zinc-blende to the tetragonal phase although the nearest-neighbor distance increases slightly. A much larger increase in R_1 occurs at the transition to the NaCl structure, where the coordination increases from 4 to 6. The mean-square deviation in the nearest-neighbor bond length, σ_1^2, appears to be a fairly smooth function of nearest-neighbor distance, decreasing (or increasing) as R_1 decreases (or increases) more or less independent of structure. Evidence from the literature was presented to suggest that the zinc-blende to tetragonal transition in CuBr (and also CuCl) should occur by shear deformation. The zinc-blende lattice becomes unstable under pressure due to a decrease in the bond-bending force constant. This mechanism is consistent with the results of our EXAFS study. Unfortunately, the information obtained from the EXAFS, even at low temperature, was not sufficient to solve completely the structure of the tetragonal phase.

I. INTRODUCTION

This work is a continuation to high pressure of an extended x-ray-absorption fine-structure (EXAFS) study of CuBr by the present authors (hereafter called I).[1] In I the anharmonic properties of CuBr were obtained by means of a temperature-dependent study. This material also has interesting x-ray-absorption properties at high pressures because the Cu and Br K edges are at convenient energies and CuBr exhibits several structural phase transitions within an accessible range of pressures. The phase diagram[2,3] for cuprous bromide is shown in Fig. 1. At standard temperature and pressure it forms in the covalent zinc-blende-structure phase, III, while at high pressures it eventually transforms to the ionic NaCl structure phase, VI.

X-ray diffraction measurements[2] indicate that the intermediate phase V probably has a tetragonal structure but are not sufficient to determine more than lattice parameters. It is not clear whether phase IV is actually a separate, homogeneous phase. The phase diagram of CuBr is almost identical to that of CuCl, a compound which has been the subject of a good deal of interest in recent years following reports[4,5] of anomalous diamagnetism in samples held under pressure and subjected to rapid temperature changes. EXAFS measurements can provide information about the short-range structure in the various phases, showing how they are related and possibly allowing identification of the crystal structure in the tetragonal phase. Analysis of the XANES may yield complementary knowledge about the geometrical and electronic structure.

Our initial work on CuBr was confusing; the apparent compressibility measured by EXAFS was much less than that determined from volume change measurements.[6] We now know that anharmonicity (as described in I) is the main cause of the discrepancy. To get a better understanding of how to interpret the CuBr data, we have also studied ZnSe. This latter compound also has the zinc-blende structure but is considerably more harmonic.

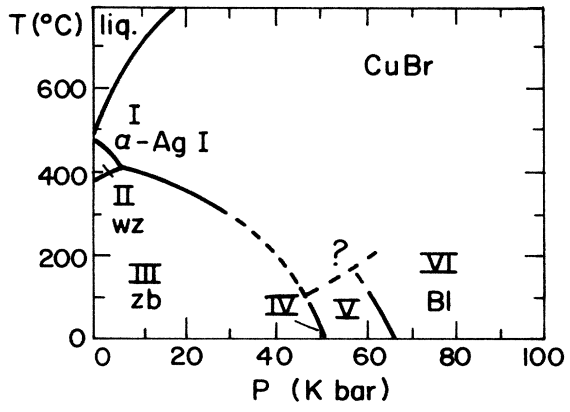

FIG. 1. Phase diagram of CuBr (taken from Ref. 3).

Analysis of the ZnSe data served as a test of the quality of the high-pressure data and of the precision which can be obtained for the various quantities determined in the data analysis. A brief description of both the ZnSe and CuBr results has recently appeared.[7]

II. EXPERIMENT

The high-pressure technique used here has been previously described.[8] Useful high-pressure studies require accurate measurements of the sample pressure. We have chosen to determine the sample pressure through the use of a calibrant material. Changes in the nearest-neighbor distance in the calibrant determined from EXAFS measurements are compared with compressibility data to determine the pressure. An ideal calibrant for high pressure EXAFS work should have a large compressibility, an open structure with no structural transitions over the pressure range of interest, no edge overlaps with the sample, a small x-ray-absorption thickness at the sample edges, and accurate compressibility data available. The alkali halide NaBr seemed to satisfy these criteria quite well and preliminary work[8] indicated that EXAFS measurements of compressibility were in good agreement with volume compressibility data. Of course NaBr cannot be used with CuBr, and so we turned to RbCl. There is a disadvantage in using RbCl because it transforms from the $B1$ to the $B2$ structure at ~ 5 kbar, and in the latter structure the first and second shells are closely spaced, complicating the EXAFS analysis. A further complication, which was only appreciated more recently, is the significant anharmonic behavior of both compounds. Unfortunately, the anharmonicity is related to the small bulk modulus and will probably be significant for any highly compressible material. (However, because of the decreased thermal damping, the EXAFS signal will extend to high k in a more harmonic solid, making possible greater precision in distance change measurements and at least partially compensating for the lower compressibility.) In spite of these problems, NaBr and RbCl have provided useful calibration results.[9] The analysis of the calibration measurements will be discussed in detail in a future work.[10]

Four samples of CuBr plus RbCl were studied using various wiggler beam lines at Stanford Synchrotron Radiation Laboratory. Each sample was held in a gasket made of Inconel 601 (annealed, in most cases) with the sample hole having a diameter of 0.79 mm (no. 68 drill). In preparing the samples, the sample and calibrant were mixed with epoxy separately, a disk of each was mounted in the gasket, and the remaining space was filled with either epoxy or silicone grease. All measurements were made at room temperature except for sample no. 4 which was measured in the clamped pressure cell and cooled with liquid nitrogen. The atmospheric pressure data described in I and room-temperature measurements on a $CuBr_2$ reference sample involved powdered samples rubbed onto several layers of Scotch Magic tape.

The CuBr powder used for sample nos. 1 and 2 came from Apache Chemical (99.999% pure). The powder was light green in color and had been sitting on the shelf for several years. Although x-ray powder diffraction patterns indicated the presence of only the pure zinc-blende structure, comments such as those of Eccles[11] on the purification of CuCl samples caused some concern about the quality of our samples. CuCl, and presumably CuBr also, is white when freshly prepared, but turns light green after prolonged exposure to the atmosphere. A second batch of CuBr obtained form CERAC (99.999% pure) was also light green in color and was used for sample nos. 3 and 4. If the light green color is evidence of surface contamination, it should have little effect on the x-ray-absorption measurements which are fairly insensitive to surface contributions. X-ray diffraction measurements suggest that this is the case, and measurements on purified samples are expected to give results very similar to those reported here.

III. RESULTS AND DISCUSSION

A. XANES analysis

The Cu and Br K edge x-ray-absorption near-edge structure (XANES) in CuBr is strongly affected by the structural phase transitions which occur at high pressure. To properly understand the relationships between the edge structures for the different phases it is important to have a good energy scale calibration. As described in I, reference edges, at standard temperature and pressured used for this purpose were the Ni K edge of nickel foil and the Bi L_3 edge of a bismuth foil. This method was applied to the measurements on sample no. 2, and the shifts in the first inflection point at each edge (relative to atmospheric pressure) are listed in Table I. Such shifts are all fairly small, but consistent trends do seem to appear. In this work the photoelectron energy origin is fixed at the first inflection point at a given pressure according to the calibration.

Typical K edge XANES (normalized to the edge step) in the zinc-blende, tetragonal, and NaCl structures of CuBr are shown in Fig. 2. At both the Cu and Br edges the white line is decreased in amplitude in the intermediate phase relative to the low- and high-pressure phases. The changes within ± 7 eV of the Cu edge seem to be mainly changes in amplitude, with only slight shifts in position of the white line. The Br edge, on the other hand, exhibits measurable shifts in the white-line position due to the phase transitions.

The normalized white-line height measured as a function of pressure is a useful measure of phase transitions in

TABLE I. Shifts in the first inflection point at the Cu and Br K edges in CuBr as a function of pressure.

		ΔE (eV)	
P (kbar)	Phase	Cu edge	Br edge
0	III	0.0±0.2	0.0±0.2
52	V	−0.1±0.2	−0.5±0.2
61	V	0.0±0.2	−0.5±0.2
68	V + VI	0.2±0.2	−0.2±0.2
77	V + VI	0.2±0.2	−0.2±0.2
87	VI	0.2±0.2	−0.1±0.2

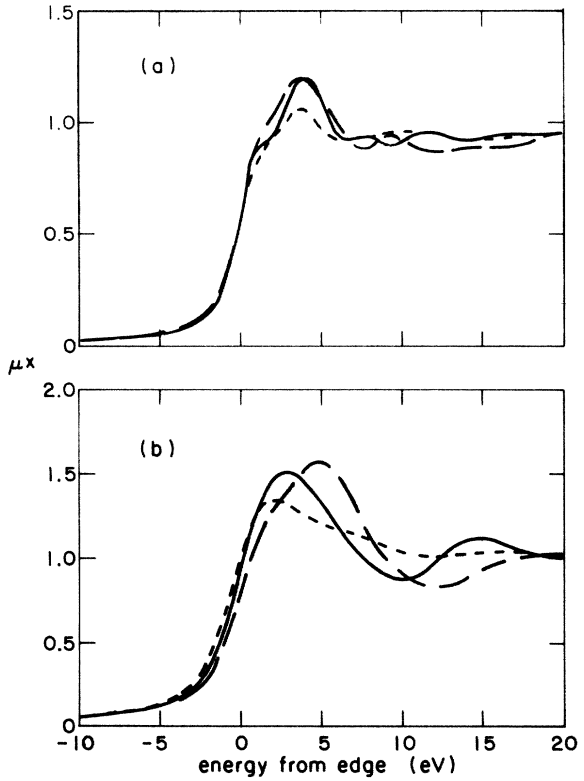

FIG. 2. Typical K edge XANES in CuBr at the (a) Cu edge and (b) Br edge. Solid line, $P=0$ kbar; dotted line, $P=56$ kbar; dashed line, $P=87$ kbar. μx has been normalized to the edge step.

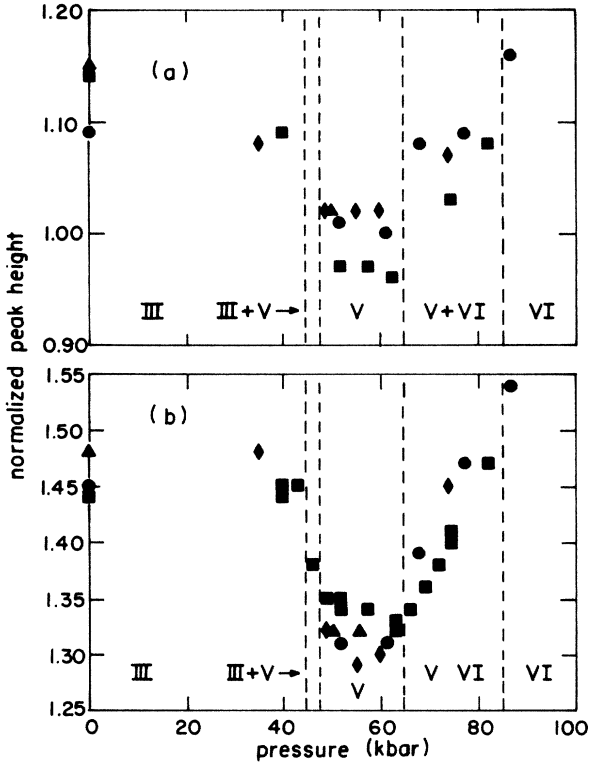

FIG. 3. Normalized white-line heights in CuBr as a function of pressure for the (a) Cu edge and (b) Br edge. Squares, sample no. 1; circles, sample no. 2; triangles, sample no. 3; diamonds, sample no. 4. The phases present in each region are indicated by Roman numerals.

CuBr. Data for the Cu and Br K edges are plotted in Fig. 3. The extra points plotted for the Br edge are from scans of the edge region which were made in order to monitor the phase transitions. The vertical dashed lines in the figure indicate the estimated boundaries between single- and mixed-phase regions. The III-V transition is observed to occur at 46 ± 5 kbar and takes place over a fairly narrow pressure range. The middle of the V-VI mixed-phase region, which is quite broad in comparison, is at 75 ± 6 kbar.

Some of the scatter in the points of Figs. 3(a) and 3(b) is probably due to errors in normalization and differences in energy resolution. However, part of the difference between samples in phase V seems to be a real effect reflecting slight differences in the edge structures. The reason for variations between different measurements is not clear. This problem will be discussed further in the EXAFS analysis section.

We find no evidence for a phase IV. X-ray diffraction[12] and optical[13] studies also found no sign of it. We believe that the alleged phase IV which has been observed in a narrow region between phases III and V in optical studies of ungasketed samples is caused or enhanced by pressure gradients. A similar "phase" has been observed in CuCl and was stabilized by using a nonhydrostatic environment.[14] The effect of CuCl has been interpreted as transient disproportionation (see Sec. III B). Whatever the explanation, the mechanism responsible for the transition phase in CuCl is probably quite similar to that in CuBr. It does not appear to be a separate, homogeneous phase.

B. Disproportionation under pressure

As mentioned in Sec. I, the high-pressure behavior of CuCl has received considerable attention in the last few years. The observations of diamagnetic anomalies, along with a report of a high-pressure metallic phase,[15] caused some speculation that CuCl might be a high-temperature superconductor. However, more recent studies[13,14,16–18] measuring the optical, electrical, and structural properties of CuCl over a wide range of pressures and temperatures conclusively show that pure CuCl has no metallic phase, and there was no indication of superconductivity at temperatures as low as ~ 10 K.[15] Another suggested explanation for the anomalous observations is that CuCl may undergo the disproportionation reaction $2\mathrm{CuCl} \rightarrow \mathrm{Cu} + \mathrm{CuCl_2}$ under pressure.[19] The presence of metallic Cu might explain metal-like resistivities. An optical-absorption feature observed at the III-IV phase transition (see Fig. 1) has been interpreted as evidence of cupric ions, but the argument is not totally convincing.[14]

Because of the similarities between the phase diagrams of CuCl and CuBr, one might expect that observations on

one of the compounds should apply to the other. If disproportionation occurs in CuCl, an analogous reaction might also occur in CuBr and vice versa. Direct evidence for disproportionation in CuBr under pressure was obtained in an energy-dispersive x-ray diffraction study.[12] Four separate samples were observed at pressures up to the V-VI transition region (70 kbar). In two of the four samples, upon releasing pressure a new set of diffraction lines corresponding to $CuBr_2$ was observed. No contribution from Cu metal was found. During a later run, repeated attempts to reproduce these observations were unsuccessful.

If disproportionation actually occurs in CuBr, its byproducts should be clearly observable with x-ray-absorption spectroscopy. In order to know what to look for, we measured the Cu and Br K edge XANES in $CuBr_2$ at atmospheric pressure. The results were compared with the edge structures observed in CuBr and Cu metal. The chemical shifts at the Cu edge were quite large and the edge structures qualitatively very different for the three materials. A distinctive low-energy bump appeared at the Br edge in $CuBr_2$ and should easily have betrayed the presence of this compound in a CuBr sample. We looked for disproportionation in two different samples. Sample no. 3 was pressurized up to 56 ± 5 kbar; upon releasing the pressure to 34 kbar, the Cu and Br edge XANES were found to look no different than the usual high-pressure zinc-blende edge structures. Sample no. 4 was taken up to 74 ± 6 kbar—well into the V-VI mixed-phase region. Even after returning the pressure to zero, there was absolutely no indication of any $CuBr_2$ in the data. The XANES obtained in the high-pressure phases did not seem to show any signs of $CuBr_2$ either. Assuming that disproportionation can occur in CuBr, it seems to be a difficult reaction to study.

C. EXAFS analysis

Let us recall that the EXAFS interference function $\chi(k)$ consists of a superposition of terms of the following type for each neighbor shell, j:

$$\chi(k)=C(k)\sin\Phi(k)\ , \tag{1}$$

with

$$C(k)=\frac{N}{kR^2}F(k)e^{-2R/\lambda}Q(k) \tag{2}$$

and

$$\Phi(k)=2kR+\delta(k)+\phi(k)\ , \tag{3}$$

where k is the photoelectron wave number, N is the coordination number for the shell, R is its distance, $F(k)$ is the corresponding backscattering amplitude, $\delta(k)$ is the net scattering phase shift, and λ is the mean free path. The quantity $Q(k)\exp[i\Phi(k)]$ describes the effects of thermal and configurational averages on the single absorption site result. In comparing two Fourier-filtered, single-shell data sets for the same sample at two different pressures, a and b, one obtains the logarithm of the amplitude ratio corresponding to a given shell,

$$\ln\left[\frac{C_a(k)}{C_b(k)}\right]=\ln\left[\frac{N_aR_b^2}{N_bR_a^2}\right]-\frac{2\,\Delta R}{\lambda}-2\,\Delta\sigma^2k^2+\frac{2}{3}\Delta\sigma^{(4)}k^4+\cdots \tag{4}$$

and the phase difference

$$\Phi_a(k)-\Phi_b(k)=2k\,(\Delta R-\Delta R_{\sigma^2})-\tfrac{4}{3}\Delta\sigma^{(3)}k^3\cdots\ , \tag{5}$$

where

$$\Delta R_{\sigma^2}=\frac{2\,\Delta\sigma^2}{R}\left[1+\frac{R}{\lambda}\right] \tag{6}$$

and where σ^2 is the mean-square deviation in bond length, and $\sigma^{(3)}$ and $\sigma^{(4)}$ are higher cumulants of the pair distribution function as discussed in I. The measured distance change is $\Delta R'=\Delta R+\Delta R_{\sigma^2}$. In all of the EXAFS analysis reported here, it has been assumed that the backscattering amplitudes $F_j(k)$ and net scattering phase shifts $\phi_j(k)$ for a particular compound are independent of small volume changes. If there are any volume-dependent effects they should be most important at low k where the photoelectrons are sensitive to the valence charge distribution and where corrections for curvature of the photoelectron wave may be substantial. However, the largest changes in interatomic spacing are less than 10% so that volume effects in $F_j(k)$ and $\phi_j(k)$ should be minimal. In future work experimental and theoretical test of this assumption should be performed.

The EXAFS function $\chi(k)$ was extracted from Cu and Br K edges, as described in I, with a cubic spline. Some typical $k^3\chi(k)$ data representative of the three phases observed are presented in Fig. 4. For the zinc-blende and tetragonal phases this quantity was qualitatively similar because in each case $\chi(k)$ is dominated by the first-shell contribution. In going to the NaCl structure a large decrease in amplitude is accompanied by the appearance of some interference from a second shell. Differences between the three phases become more apparent when one looks at the Fourier transforms[20] of $k^3\chi(k)$, which are plotted in Fig. 5. The first-shell peak behaves identically in both the Cu and Br edge transforms: it decreases in amplitude and shifts to higher r in each successive phase. Beyond the first shell in the Br edge transforms, a second shell is barely visible near 4 Å in the zinc-blende phase. Second- and third-shell peaks appear at lower r in the tetragonal phase, while a large second shell is present in the rocksalt structure. In the Cu edge transforms, peaks beyond the first are almost nonexistent in the first two phases. In the NaCl structure, the third-shell peak is larger than the second. This behavior is due to the large Cu-Cu relative motion discussed in I.

It is convenient to begin the quantitative analysis by considering the behavior of the first-shell distribution in the single-phase data. First shell $\chi(k)$ were isolated with a typical r-space window of 1.3 to 2.8 Å. (The window was shifted as necessary.) The change in nearest-neighbor distance was determined using the 72 K, atmospheric pressure data as reference. The phase differences were fit

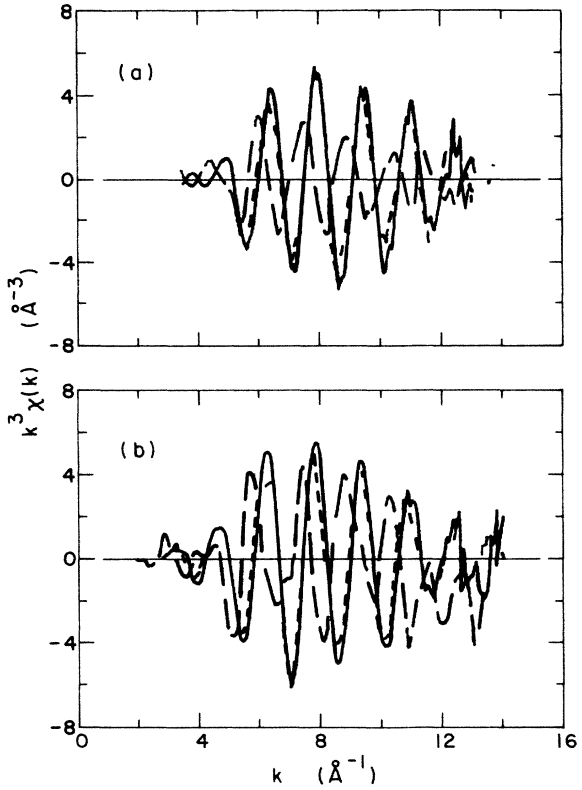

FIG. 4. Typical $k^3\chi(k)$ data for CuBr: (a) Cu edge data, (b) Br edge data. Solid line: sample no. 1, $P=40$ kbar; dotted line: sample no. 1, $P=52$ kbar; dashed line sample no. 2, $P=87$ kbar.

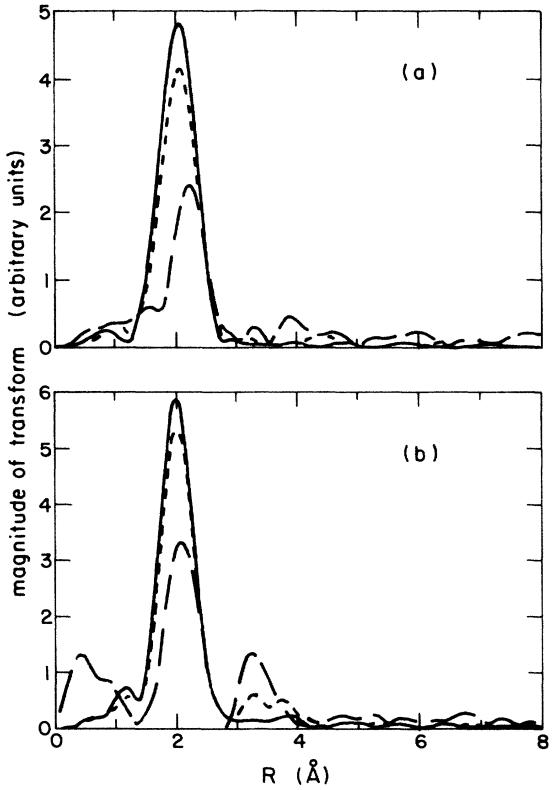

FIG. 5. Magnitudes of Fourier transforms of $k^3\chi(k)$ for CuBr: (a) Cu edge data, (b) Br edge data. Solid line: sample no. 1, $P=40$ kbar; dotted line: sample no. 1, $P=52$ kbar; dashed line: sample no. 2, $P=87$ kbar.

with a straight line and with a polynomial including a k^3 term; both fits were forced to pass through the origin. In all cases the quality of the straight-line fits (as measured by χ^2) was very poor and the cubic term was seen to be necessary for a satisfactory description of the data. The results of the two sets of fits for the Cu and Br edge data are listed in Table II. The straight-line results are included just for comparison. The differences between Cu and Br edge results give an idea of the uncertainties in the parameters. These differences are about the same size of those seen in ZnSe between Zn and Se edge data in similar fits. Shifting the energy origin of a data set relative to that of the reference by 0.3 eV causes ΔR and $\sigma^{(3)}$ to change by 0.003 Å and 0.03×10^{-3} Å^3, respectively.

Some typical phase differences together with the anharmonic fits are plotted in Fig. 6. The range of points used

TABLE II. Results of least-squares fits to phase-difference data for CuBr.

Sample no.	P (kbar)	$\Delta R'$ (Å) Cu	$\Delta R'$ (Å) Br	$\Delta R'$ (Å) Cu	$\Delta R'$ (Å) Br	$\sigma^{(3)}$ (10^{-3} Å^3) Cu	$\sigma^{(3)}$ (10^{-3} Å^3) Br
1	0.0	−0.025	−0.022	−0.006	−0.012	0.41	0.23
	39.9	−0.064	−0.069	−0.050	−0.062	0.39	0.14
	51.7	−0.047	−0.051	−0.020	−0.039	0.64	0.22
	57.4	−0.048	−0.052	−0.026	−0.043	0.48	0.20
	62.6	−0.055	−0.059	−0.038	−0.049	0.44	0.23
2	0.0	−0.013	−0.021	−0.011	−0.011	0.05	0.50
	51.7	−0.024	−0.033	0.008	−0.022	0.81	0.24
	61.1	−0.036	−0.037	−0.004	−0.022	0.70	0.39
	86.6	0.069	0.075	0.079	0.107	0.29	0.86
4	35.0	−0.062	−0.062	−0.050	−0.043	0.20	0.37
	48.8	−0.018	−0.021	0.017	0.001	0.65	0.56
	55.1	−0.018	−0.026	0.015	−0.015	0.84	0.31
	59.7	−0.029	−0.027	0.009	−0.013	0.78	0.47

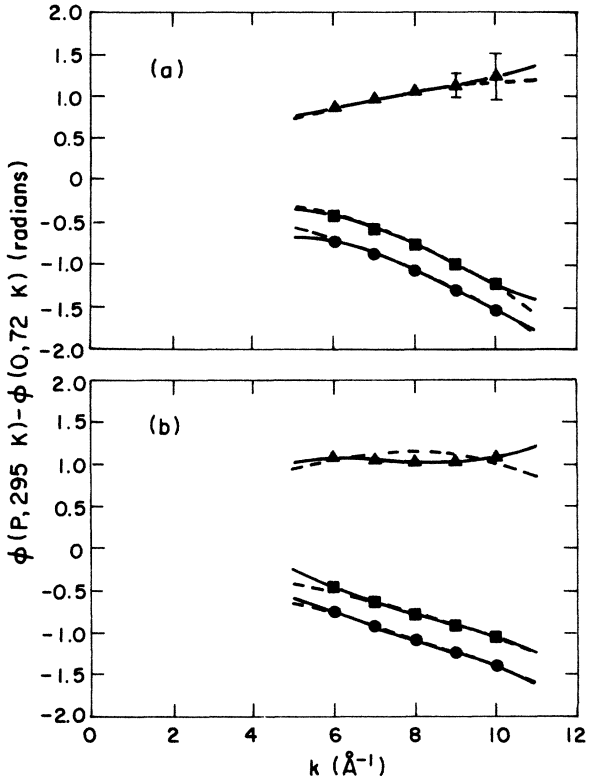

FIG. 6. Typical first-shell phase differences for CuBr: (a) Cu edge data, (b) Br edge data. Circles: sample no. 1, $P=40$ kbar; squares: sample no. 1, $P=52$ kbar; triangles: sample no. 2, $P=87$ kbar. The dashed lines represent least-squares fits to the data.

in the fits (6—10 Å^{-1}) had to be restricted for two reasons. At low k there is a large, sharp dip in both the Cu and Br backscattering amplitudes which is greatly distorted by the relatively narrow r-space window. At the other end of the k range the single-shell amplitude becomes quite small and is often dominated by noise contributions, resulting in unreliable phase-difference and amplitude-ratio results. Within the fitting range distortions of the phase and amplitude can also occur, and they have large effects on the parameters obtained in anharmonic fits. The parameters in the anharmonic fitting polynomials are highly correlated so that, for example, a large error in $\sigma^{(3)}$ results in a large error in ΔR. All of this discussion is meant to explain why, although anharmonic terms are required to give a satisfactory description of phase differences and amplitude ratios, the errors in the fitted values may be quite large. Allowing more than two degrees of freedom in each fit will give unreasonable and meaningless results for the fitting parameters.

Since $\sigma^{(3)}$ appears to be significant at all pressures, one may expect $\sigma^{(4)}$ to be important also. This fact complicates the analysis of amplitude ratios for phase-V data because the coordination number in this phase is not known *a priori* and it is not practical to determine N/N_0, σ^2, and $\sigma^{(4)}$ in the same fit. It is possible to make some assumptions about N and to then see if they are consistent with the data. We know that CuBr starts in the zinc-blende phase, where $N=4$, and ends up in the rocksalt structure when $N=6$. It seems likely that any intermediate structure would also have a coordination of either 4 or 6. After looking at a few amplitude ratios one is quickly convinced that the first-shell coordination number in phase V is 4. Some typical amplitude ratios, corrected for the change in nearest-neighbor distance, for all three observed phases are shown in Fig. 7. The anharmonic fits shown all pass through the origin (the reference data has $N=4$). The ratio for the NaCl structure data has been corrected for the increase in coordination number from 4 to 6. (The difference in the ratios for Cu and Br edge data at the highest pressure are probably due to distortion of the Br data at high k—the amplitude is quite small in this region.)

Using the above conclusions about coordination numbers, the amplitude ratios were analyzed with the usual straight-line and anharmonic fits. The results are listed in Table III. Although the inclusion of $\sigma^{(4)}$ generally causes significant improvement of the fits, the correlation between $\Delta\sigma^2$ and $\sigma^{(4)}$ together with various distortions probably leads to large errors in the values obtained. A change in the y intercept of 0.05 causes $\Delta\sigma^2$ and $\sigma^{(4)}$ to increase by 0.1×10^{-2} Å^2 and 0.2×10^{-4} Å^4, respectively.

With $\Delta\sigma^2$ determined, the $\Delta R'$ values can be corrected to give the change in nearest-neighbor distance as a func-

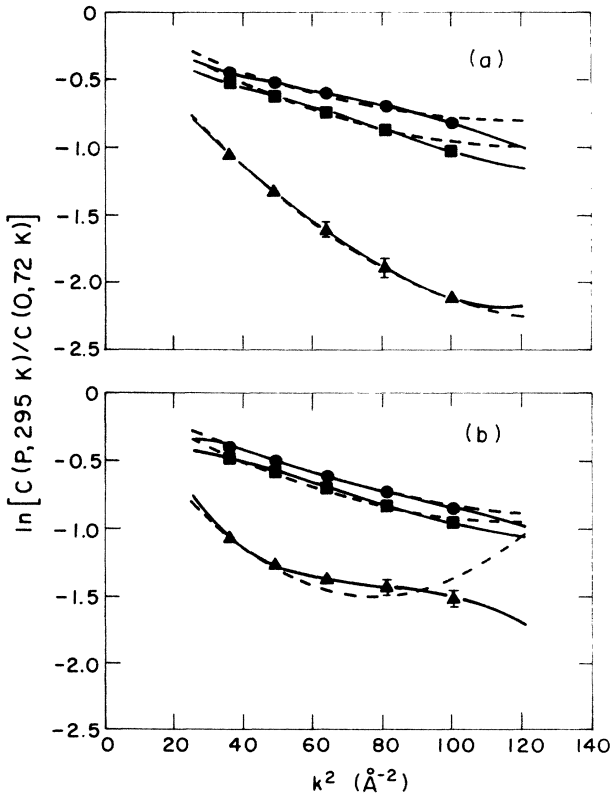

FIG. 7. Typical first-shell amplitude ratios, corrected for distance changes, for CuBr: (a) Cu edge data, (b) Br edge data. Circles: sample no. 1, $P=40$ kbar; squares: sample no. 1, $P=52$ kbar; triangles: sample no. 2, $P=87$ kbar. The dashed lines represent least-squares fits to the data.

TABLE III. Results of least-squares fits to amplitude ratios for CuBr.

Sample no.	P (kbar)	$\Delta\sigma^2$ (10^{-2} Å^2) Cu	$\Delta\sigma^2$ (10^{-2} Å^2) Br	$\Delta\sigma^2$ (10^{-2} Å^2) Cu	$\Delta\sigma^2$ (10^{-2} Å^2) Br	$\sigma^{(4)}$ (10^{-4} Å^4) Cu	$\sigma^{(4)}$ (10^{-4} Å^4) Br
3	0.0	0.76	0.73	0.96	0.89	1.12	0.77
3	39.9	0.51	0.50	0.68	0.62	0.86	0.61
3	51.7	0.60	0.58	0.80	0.78	0.96	0.95
3	57.4	0.60	0.56	0.76	0.81	0.82	1.12
3	62.6	0.53	0.58	0.82	0.82	1.14	1.24
4a	0.0	0.78	0.69	0.94	0.90	1.06	1.03
4a	51.7	0.63	0.57	0.80	0.85	0.69	1.14
4a	61.1	0.59	0.63	0.83	0.80	0.90	0.92
4a	86.6	1.28	1.44	1.66	1.96	1.81	3.80
5b	35.0	0.54	0.48	0.81	0.56	1.10	0.48
5b	48.8	0.60	0.53	0.87	0.65	1.36	0.52
5b	55.1	0.54	0.51	0.68	0.62	0.74	0.54
5b	59.7	0.55	0.55	0.65	0.59	0.58	0.22

tion of pressure at room temperature. The corrections for thermal expansion between the 72-K sample and room-temperature sample ($=0.006$ Å) and ΔR_{σ^2} cancel out almost completely in most cases. (As in I, the value of λ in Eq. (6) was taken to be 8 Å.) The resulting ΔR values are plotted in Fig. 8 as a function of pressure. Within each structural phase the nearest-neighbor distance decreases with pressure, but at the transitions there are large increases in distance. For comparison, the solid line represents the measurements of Vaidya and Kennedy[21] and the crosses indicate the results of an energy-dispersive x-ray diffraction study.[22] The star indicates the NaCl structure result measured with x-ray diffraction by Meisalo and Kalliomaki.[2] The EXAFS results in the zinc-blende phase are more or less consistent with the other measurements considering the errors due to the anharmonic fitting. In the tetragonal phase, the scatter among data points from the same sample are consistent with measurement uncertainties; however, the average differences between samples appear to be real, as is discussed later.

To interpret the $\Delta\sigma^2$ results, it is convenient to convert them to the relative change in σ^2 at room temperature and plot them as a function of the relative change in nearest-neighbor distance. To make the conversion, the measured value of $\Delta\sigma^2=0.0080$ Å^2 between 295 and 72 K and the calculated value σ^2 (72 K)$=0.0037$ Å^2 were used (see I); the results are plotted in Fig. 9. There is clearly quite a bit of scatter, but the data seem to follow a consistent trend: σ^2 decreases as the nearest-neighbor distance decreases, more or less independent of structure. The large increase of σ^2 in going to the NaCl structure can easily be understood in this way. Raman measurements[23] indicate that the Grüneisen parameter, γ_E, for the TO mode in

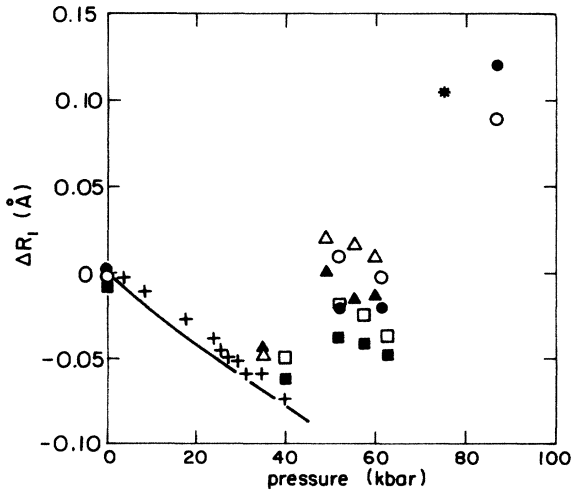

FIG. 8. Change in nearest-neighbor distance vs pressure for CuBr. Squares, sample no. 1; circles, sample no. 2; triangles, sample no. 4. Open (solid) symbols represent Cu (Br) edge data. The solid line is from Ref. 18, the crosses are from Ref. 19, and the star is from Ref. 2.

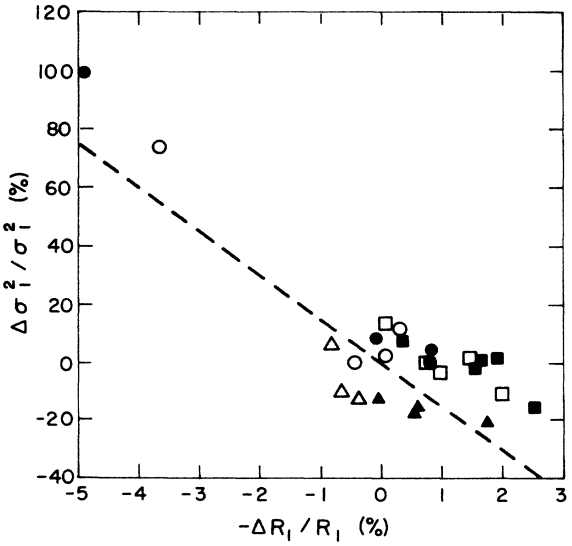

FIG. 9. Δ_1^2/σ_1^2 vs $-\Delta R_1/R_1$ for CuBr. Squares, sample no. 1; circles, sample no. 2; triangles, sample no. 4. Open (solid) symbols represent Cu(Br) edge data. The dashed line is explained in the text.

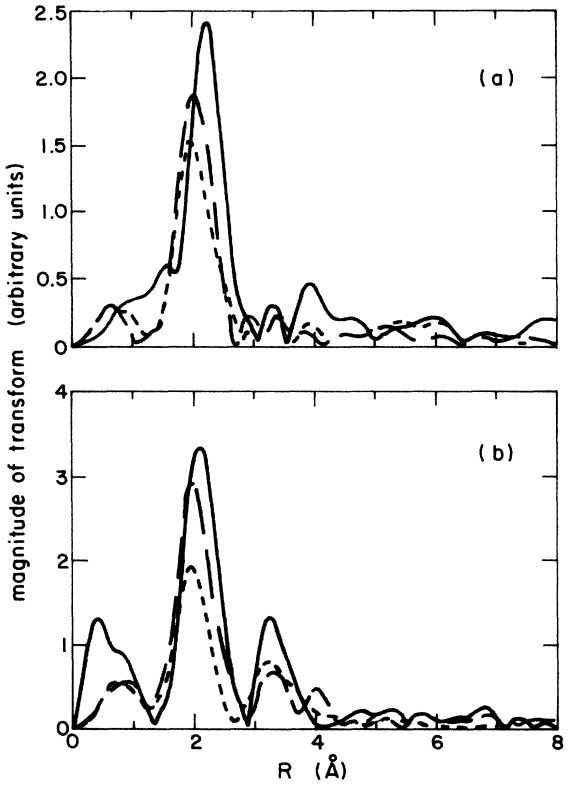

FIG. 10. Magnitudes of Fourier transforms of $k^3\chi(k)$ for CuBr (sample no. 2) in the V-VI mixed-phase region: (a) Cu edge data, (b) Br edge data. Dashed line, $P=68$ kbar; dotted line, $P=77$ kbar; solid line, $P=87$ kbar.

CuBr is approximately 2.5. Setting γ_E equal to this value and using[7] $\Delta\sigma^2/\sigma^2=6\gamma_E(\Delta R/R)$ gives results corresponding to the dashed line in the figure.

Analysis of the second shell in the Br edge data affords good evidence that the $P=87$ kbar data of sample no. 2 corresponds to the NaCl structure. This data was filtered with an r window of 2.9 to 3.9 Å and compared with the filtered second shell $\chi(k)$ from the 73 K, zero-pressure data. A linear fit to the phase difference gave $\Delta R_2=-0.39\pm0.03$ Å which, combined with the averaged result for the first shell, gives $R_2/R_1=3.62/2.56=1.414\simeq\sqrt{2}$ as expected for the NaCl structure. A straight-line fit to the logarithm of the ratio of amplitudes yields an intercept $a_0=-0.17\pm0.15$ and $\Delta\sigma^2=0.0070\pm0.0020$ Å^2. The intercept result is consistent with a second-shell coordination which is the same as in the zinc-blende structure. Both the rocksalt and zinc-blende structures are fcc with a basis and hence have a second-shell coordination of 12.

Figure 10 shows some Fourier transforms of $k^3\chi(k)$ measured in the V-VI mixed-phase region. Interference between first-shell contributions from the two phases causes the amplitude of the first-shell peak to be greatly reduced in the mixed-phase region. At the same time, one can see that the second-shell peak in the Br edge data, corresponding to the second shell in the NaCl structure, steadily increases in amplitude. To analyze this data it was necessary to resort to nonlinear least-squares fitting. The first-shell peak was filtered in the usual way to obtain single-shell $\chi(k)$ data. The reference data for fitting were filtered first shell $\chi(k)$ which were pure phase V and phase VI. Sample no. 2, $P=87$ kbar, was used as the phase-VI reference in all cases, while sample no. 1, $P=63$ kbar and sample no. 2, $P=61$ kbar were the phase-V references for the respective samples. It was assumed that every atomic site in the mixed-phase sample was in one phase or the other, so that

$$\chi(\mathrm{V+VI})=f(\mathrm{V})\chi(\mathrm{V})+f(\mathrm{VI})\chi(\mathrm{VI}) \tag{7}$$

with

$$f(\mathrm{V})+f(\mathrm{VI})=1\ . \tag{8}$$

This model gives one fitting parameter, which was taken to be f(VI). Good fits were obtained without allowing R_1 values to vary, but it was necessary to include a parameter $\Delta\sigma^2$(VI). The results for all of the mixed-phase data analyzed are presented in Table IV. A graphical presentation of the f(VI) results is given in Fig. 11. Uncertainties in the parameters are difficult to assess, especially considering the correlation between f(VI) and $\Delta\sigma^2$(VI). It is worthwhile noting, however, that the results of fitting the mixed phase $\chi(k)$ are in good agreement with the trend shown by the normalized white-line peak height in the same pressure region (see Fig. 3).

We now return to a consideration of phase V. It was noted earlier that some variations have been observed in the Cu and Br edge XANES measured in the tetragonal phase for different samples. Some variations also occur in the EXAFS data: the first shell appears to be fairly consistent between the different samples, but the higher shells, which are really only visible in the Br edge data, vary considerably. This inconsistency is unfortunate since information beyond the first shell is necessary in order to

TABLE IV. Results of nonlinear least-squares fits to $\chi(k)$ for CuBr data in the V-VI mixed-phase region.

Sample no.	P (kbar)	f(VI) Cu	f(VI) Br	$\Delta\sigma^2$(VI) (10^{-2} Å^2) Cu	$\Delta\sigma^2$(VI) (10^{-2} Å^2) Br
3	74.4	0.42	0.36	0.95	1.42
3	82.0	0.65		0.11	
4a	68.0	0.51	0.40	0.78	1.22
4a	77.2	0.66	0.64	0.56	0.68

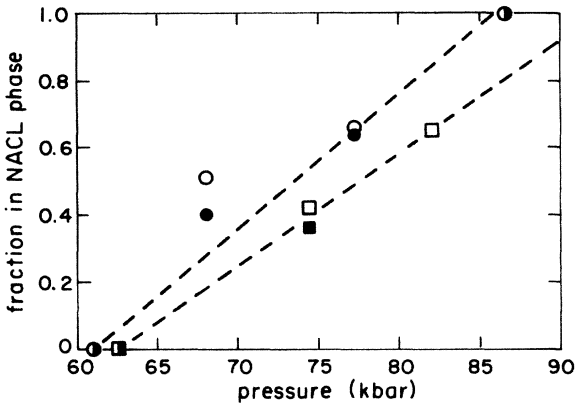

FIG. 11. Fraction of CuBr sample in phase VI as a function of pressure. Squares, sample no. 1; circles, sample no. 2. Open (solid) symbols represent Cu (Br) edge data. The dashed lines are merely guides to the eye.

determine the crystal structure. Besides this problem, the higher shells observed at room temperature are quite small in amplitude so that little useful information can be obtained from them.

To decrease the thermal damping of the higher shells, we loaded sample no. 4 in the clamped cell and cooled it. By pouring liquid nitrogen directly onto the cell we were able to cool the ring centering the sample gasket to ~ 100 K, but at the lowest temperatures there was a variation of ~ 20 K during each scan due to evaporation of the coolant. Fourier transforms of data collected at several different temperatures are displayed in Fig. 12. Several shells show the expected increase in amplitude as the temperature decreases. The pressure at room temperature was 49 kbar, although it may be varied at lower temperatures. In spite of the sample-to-sample variations mentioned above, we have attempted an analysis of the low-temperature data.

Individual shells in the lowest temperature data for each edge were filtered and analyzed with the phase difference and amplitude ratio methods, using the filtered first and second shell $\chi(k)$ from the 72 K, atmospheric pressure data as reference. As usual, the most reliable information was obtained about the first shell. For the Br edge the results were $\Delta R = -0.001 \pm 0.003$ Å and, for the amplitude ratio fit, $a_0 = 0.04 \pm 0.05$ and $\Delta\sigma^2 = 0.0005 \pm 0.0010$ Å^2. These results are consistent with the room-temperature first-shell analysis. The Cu edge first shell showed some strange features, however. The amplitude showed a large dip and the phase increased rapidly at low k relative to the reference. The only plausible explanation for these features seems to be interference from a second shell. Since similar behavior does not appear in the Br edge data, the extra contribution must be a Cu-Cu shell. A reasonable fit to the data was obtained by using a 4-atom Cu-Br shell at $R = 2.46$ Å and a Cu-Cu shell at 2.78 ± 0.02 Å. The number of atoms in the Cu-Cu shell is difficult to determine because of the correlation between N and σ^2, but at least four seems to be needed to give a reasonable fit.

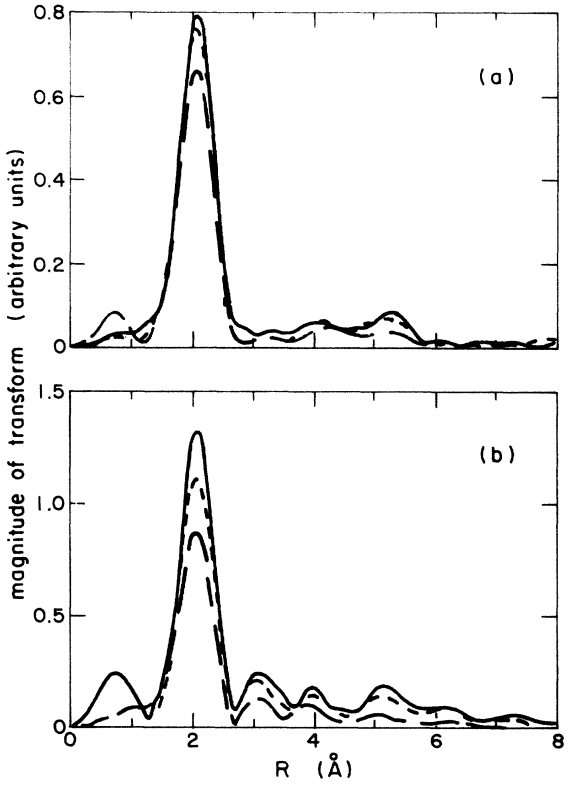

FIG. 12. Magnitudes of Fourier transforms of $k^2\chi(k)$ for CuBr-V at low temperatures: (a) Cu edge data: solid line, $T \sim 130$ K; dotted line, $T \sim 145$ K; dashed line, $T \sim 205$ K. (b) Br edge data: solid line, $T \sim 100$ K; dotted line, $T \sim 130$ K; dashed line, $T \sim 215$ K.

Limited information could be obtained about the higher shells. Because of the small amplitudes of the shells and the similarities between the backscattering properties of Cu and Br atoms, it is very difficult to pin down the atomic species in a given shell. Furthermore, what appears to be a single shell may actually be several closely spaced shells of more than one kind of atom. Analysis of the amplitudes could give misleading results, so only the positions of shells will be discussed here. The error in distance obtained if a shell of Br atoms is assumed to be Cu, or vice versa, is 0.1 Å; this is the limit on distance resolution here. In the Br edge data, peaks are found at 3.43 ± 0.10 Å (probably Br-Br), 4.56 ± 0.10 Å, and 5.60 ± 0.10 Å. The last shell shows a beat in $\chi(k)$, so it may actually be two distinct shells with the distance given being an average of some sort. In the Cu edge data, peaks are found at 4.72 ± 0.10 Å and 5.23 ± 0.10 Å.

D. Structural phase transitions in CuBr

The stable structure at a given temperature and pressure is determined by minimizing the Gibbs free energy of the system, $G = G(P,T)$. At a phase transition the difference in free energy between two structures is given by

$$\Delta G = \Delta E(P,T) + P\,\Delta V(P,T) - T\,\Delta S(P,T) = 0 . \quad (9)$$

For temperatures sufficiently near zero one can ignore the

entropy term. In this case, the $P\Delta V$ term can make it energetically favorable for a crystal to collapse to a denser phase under pressure. That is, a crystal will transform to a structure with a higher internal energy if the corresponding increase in energy is compensated by a sufficient decrease in volume.

All tetrahedral semiconductors transform from fourfold to sixfold coordinated structures under pressure.[24,25] The elemental semiconductors transform to metallic β-Sn phases, while the ionic II-VI compounds are converted to a semiconducting NaCl structure before going metallic. The III-V compounds go directly to a metallic structure which may be the rocksalt modification or a β-Sn analogue.[26] CuCl and CuBr are very ionic and hence eventually reach the NaCl structure. However, before reaching that structure they each pass through an intermediate tetragonal phase. This extra phase does not fit the pattern set by the other tetrahedral semiconductors and, as will be shown below, is due to the instability of the zinc-blende structure under pressure and the extreme ionicity of CuCl and CuBr.

Musgrave and Pople[27] pointed out a number of years ago that the zinc-blende structure under hydrostatic pressure can become unstable with respect to shear deformations. With the coordinate axes chosen to lie along the edges of the unit cube, they considered two independent types of shearing motion: (1) $(x,y,z)\rightarrow(x+uy,y,ux,z)$ and (2) $(x,y,z)\rightarrow(x+ux,y-uy,z)$. (There are, of course, three possible permutations for each type of deformation.) In each transformation the volume changes from V_0 to $(1-u^2)V_0$. The elastic constants corresponding to these deformations are c_{44} and $c_s=\frac{1}{2}(c_{11}-c_{12})$, respectively. In terms of the elastic constants the changes in internal energy due to the two types of transformation are $2c_{44}u^2$ and $(c_{11}-c_{12})u^2$. It follows from Eq. (9) that at zero temperature a shear deformation of the zinc-blende structure will occur if

$$2c_{44}(P)-P=0 \tag{10}$$

or

$$c_{11}(P)-c_{12}(P)-P=0\ . \tag{11}$$

The elastic constant in tetrahedral semiconductors show consistent trends when considered as functions of ionicity.[28] c_s and c_{44} normalized to e^2/r^4 (with $r=R_1$) are observed to decrease with ionicity, approaching zero for the most ionic compounds CuCl and CuBr. It is informative to interpret these trends in terms of a simple force constant model. A convenient one is the special case of the valence-force-field model suggested by Keating,[29] in which the potential energy of the lattice is written as

$$U=\tfrac{1}{2}\alpha\left[\frac{3}{4r^2}\right]\sum_{i=1}^{4}[\Delta(\mathbf{r}_i^1\cdot\mathbf{r}_i^1)]^2 + \tfrac{1}{2}\sum_{s=1}^{2}\beta^s\left[\frac{3}{4r^2}\right]\sum_{i=1}^{4}\sum_{\substack{j=1\\ j>i}}[\Delta(\mathbf{r}_i^s\cdot\mathbf{r}_j^s)]^2\ , \tag{12}$$

where $\mathbf{r}_i^s$ is a bond vector about atom s. α and $\beta=\frac{1}{2}(\beta^1+\beta^2)$ can be interpreted as bond-stretching and bond-bending force constants, respectively. In terms of these force constants it can be shown[28] that, ignoring the Coulombic contributions,

$$c_{44}\sim(\alpha+\beta)/r \tag{13}$$

and

$$c_s\sim\beta/r\ . \tag{14}$$

From this model one can see that the decrease in the shear moduli is due to the decrease in the bond-bending force constant with ionicity.

Pressure also has an effect on the elastic constants. A pseudopotential calculation of the electronic properties of ZnSe as a function of volume has shown that the valence bond charges decrease under pressure, suggesting a corresponding decrease in β.[30] Ultrasonic measurements of the elastic constants in ZnSe under pressure do indeed show that $dc_s/dp=-0.17$, while $dc_{44}/dp=0.33$.[31] These ideas can be related to our own observations for ZnSe.[7] Consider σ^2 for the second shell in zinc-blende structure. A pair of second nearest-neighbor atoms must sit at the corners of a coordination tetrahedron. Since relative motion between such a pair of atoms will consist mainly of bond-bending motion, one may expect that $\sigma_2^2\sim 1/\beta$. A decrease in β should cause an increase in σ_2^2 with pressure, which is exactly what was observed. If we write

$$\frac{1}{\sigma_2^2}\frac{\Delta\sigma_2^2}{\Delta P}\approx-\frac{1}{\beta}\frac{\Delta\beta}{\Delta P}\approx-\frac{d\ln\beta}{dP}\ , \tag{15}$$

then we find $d\ln\beta/dP\approx-0.002$ kbar^{-1}, just a factor of 2 larger than the result obtained from the elastic constant measurements.

The elastic constants in CuCl change even more rapidly with pressure. The values at room temperature and atmosphere pressure, $c_s=45.5$ kbar and $c_{44}=136$ kbar, are quite small to begin with, and with pressure derivatives of -0.388 and -0.658, respectively, they decrease quickly under pressure.[32] Applying Eqs. (10) and (11) one predicts transition pressures of 82 and 51 kbar, respectively. The lower value is equal, within experimental uncertainty, to the observed zinc-blende to tetragonal phase-transition pressure in CuCl. The obvious conclusion, then, is that the II-IV transition in CuCl occurs (or at least begins) by shear deformation due to lattice instability. A similar prediction is expected to hold for the III-V transition in CuBr, although no high-pressure measurements of its elastic constants are available. In contrast, the predicted pressure for a type-2 transition in ZnSe is 265 kbar, well above the observed 137-kbar transition to the NaCl structure.[33–35]

The prediction of a transition from the zinc-blende structure to a tetragonal phase by shear deformation is in good agreement with the results of our EXAFS measurements. The III-V transition in CuBr is observed to occur fairly rapidly over a narrow pressure range. The transition to the NaCl structure, on the other hand, is quite sluggish and probably requires nucleation and growth of crystallites in the new phase. The observed first-shell distribution in phase V is also consistent with a type-2 shear deformation: the coordination remains unchanged while the distance increases slightly.

A simple shear deformation to a tetragonal or orthorhombic structure should leave a lattice with identical radial distribution functions about Cu and Br atoms (at least for coordination numbers and distances). Our high-pressure, low-temperature measurements indicate that this is not the case in CuBr-V. If the measurements and analysis are correct, some additional rearrangement of atoms must occur in the transition. This complicates analysis of the crystal structure since it cannot be viewed as just a simple deformation of the zinc-blende structure. The only practical way to proceed is to look for model structures and see if they are consistent with the EXAFS and x-ray diffraction measurements.

The most obvious choice for a model is the tetragonal phase of AgI observed between 3 and 4 kbar. AgI-IV has a structure similar to PbO, with a nearest-neighbor coordination of 4.[36] Although it is possible to explain some of the EXAFS results with this structure, it is not possible to simultaneously satisfy the requirements of both the EXAFS and x-ray diffraction measurements. This is unfortunate since it has been difficult to find other reasonable structural models. We have been unable to find any other examples of tetragonal modifications which come close to satisfying all of the data. It appears that the structure of CuBr-V will remain unsolved until more information on it can be obtained.

ACKNOWLEDGMENTS

We are happy to thank the following for their gracious assistance with the various phases of this work: E. D. Crozier, J. J. Rehr, B. A. Bunker, and J. E. Whitmore. This work was supported in part by National Science Foundation Grant Nos. DMR-78-24995 and DMR-77-27489 and by U.S. Department of Energy Grants DE-AT06-83ER45038 and DE-FG06-84ER45163. The Stanford Synchrotron Radiation Laboratory (S.S.R.L.) is supported by the U.S. Department of Energy (Office of Basic Energy Sciences) and the National Institute of Health (Biotechnology Research Program, Division of Research Resources).

[1]J. M. Tranquada and R. Ingalls, Phys. Rev. B **28**, 3520 (1983), hereafter referred to as I.

[2]V. Meisalo and M. Kalliomaki, High Temp. High Pressures **5**, 663 (1973).

[3]C. W. F. T. Pistorius, Prog. Solid State Chem. **11**, 1 (1976).

[4]N. B. Brandt, S. V. Kuvshinnikov, A. P. Rusakov, and M. V. Semenov, Pis'ma Zh. Eksp. Teor. Fiz. **27**, 37 (1978) [JETP Lett. **27**, 33 (1978)].

[5]C. W. Chu, A. P. Rusakov, S. Huang, S. Early, T. H. Geballe, and C. Y. Huang, Phys. Rev. B **18**, 2116 (1978).

[6]R. Ingalls, J. M. Tranquanda, J. E. Whitmore, E. D. Crozier, and A. J. Seary, in *EXAFS Spectroscopy: Techniques and Applications,* edited by B. K. Teo and D. C. Joy (Plenum, New York, 1981), pp. 127–128.

[7]J. M. Tranquada and R. Ingalls, in *EXAFS and Near Edge Structure III,* edited by J. O. Hodgson, B. Hedman, and J. E. Penner-Hahn (Springer-Verlag, Berlin, 1984), p. 388.

[8]R. Ingalls, E. D. Crozier, J. E. Whitmore, A. J. Seary, and J. M. Tranquada, J. Appl. Phys. **51**, 3158 (1980).

[9]J. M. Tranquada, Ph.D. thesis, University of Washington, Seattle, Washington, 1983 (unpublished).

[10]J. E. Whitmore, R. Ingalls, and J. M. Tranquada (unpublished).

[11]T. K. Eccles, Ph.D. thesis, Stanford University, 1977 (unpublished).

[12]E. F. Skelton, S. B. Qadri, A. W. Webb, R. Ingalls, and J. M. Tranquada, Phys. Lett. **94A**, 441 (1983).

[13]H. Miller, S. Ves, H. D. Hochheimmer, and M. Cardona, Phys. Rev. B **22**, 1052 (1980).

[14]B. Batlogg, J. P. Remeika, and R. G. Maines, Solid State Commun. **38**, 83 (1981).

[15]N. R. Serebryanaya, S. V. Popova, and A. P. Rusakov, Fiz. Tverd Tela (Leningrad) **17**, 2772 (1975) [Sov. Phys.—Solid State **17**, 1843 (1975)].

[16]G. J. Piermarini, F. A. Mauer, S. Block, A. Jayaraman, T. H. Geballe, and G. W. Hall, Jr., Solid State Commun. **32**, 275 (1979).

[17]E. F. Skelton, A. W. Webb, J. F. Rachford, P. C. Taylor, S. C. Yu, and I. L. Spain, Phys. Rev. B **21**, 5289 (1980).

[18]E. F. Skelton, F. J. Rachford, A. W. Webb, S. C. Yu, and I. L. Spain, Phys. Rev. B **21**, 5289 (1980).

[19]E. I. Blount and J. C. Phillips, J. Less Common Met. **62**, 457 (1978).

[20]In all cases, the k-weighted χ data were multiplied by a Gaussian centered on the data range and decaying to 10% at the edges before Fourier transforming.

[21]S. N. Vaidya and G. C. Kennedy, J. Phys. Chem. Solids **32**, 951 (1971).

[22]E. F. Skelton and S. B. Qadri (private communication).

[23]H. D. Hochheimmer, M. L. Shand, J. E. Potts, R. C. Hanson, and C. T. Walker, Phys. Rev. B **14**, 4630 (1976).

[24]J. C. Phillips, *Bonds and Bands in Semiconductors* (Academic, New York, 1973), pp. 201–204.

[25]J. A. Van Vechten, Phys. Rev. B **7**, 1479 (1973).

[26]S. Froyen and M. L. Cohen, Solid State Commun. **43**, 447 (1982).

[27]M. J. P. Musgrave and J. A. Pople, J. Phys. Chem. Solids **23**, 321 (1962).

[28]R. M. Martin, Phys. Rev. B **10**, 4005 (1970).

[29]P. N. Keating, Phys. Rev. **145**, 637 (1966).

[30]W. Andreoni and K. Maschke, Phys. Rev. B **22**, 4816 (1980).

[31]B. H. Lee, J. Appl. Phys. **41**, 2988 (1970).

[32]R. C. Hanson, K. Helliwell, and C. Schwab, Phys. Rev. B **9**, 2649 (1974).

[33]G. A. Samara and H. G. Drickamer, J. Phys. Chem. Solids **23**, 457 (1962).

[34]P. L. Smith and J. E. Martin, Phys. Lett. **19**, 541 (1965).

[35]B. A. Weinstein, in *High-Pressure Science and Technology: Sixth AIRAPT Conference,* edited by K. D. Timmerhaus and M. S. Barber (Plenum, New York, 1979), Vol. 1, pp. 141–151.

[36]M. J. Moore and J. S. Kasper, J. Chem. Phys. **48**, 2446 (1968).